Paper **3350-14**, *Proc. SPIE Astronomical Telescopes and Instrumentation Conference*, Kona Hawaii, March 1998

The Interferometry Program Flight Experiments: IPEX I&II

Marie B. Levine

Jet Propulsion Laboratory
California Institute of Technology
4800 Oak Drive, M.S. 157-316
Pasadena, CA 91109

ABSTRACT

The **I**nterferometry **P**rogram **EX**periments (IPEX) I and II are a series of flight experiments designed to characterize microdynamics of structures in space. These technology demonstration flight experiments are precursors to the Space Interferometry Mission (SIM), Next Generation Space Telescope (NGST) and Terrestrial Planet Finder (TPF), and will address the missions' nanometer-level structural stability requirements. Of particular interest is potential thermal snapping when space structures undergo rapid thermal variations, such as a sun-to-shade transition. This information is needed to characterize uncontrollable high frequency disturbances,. and to validate structural designs and modeling approaches for joint-dominated extruding structures. Another objective of the experiments is to characterize typical mechanical disturbances of spacecraft while on-orbit for the purpose of modeling and disturbance response prediction for future optical space missions. Both experiments are performed on the German DARA/DASA free-flying platform Astro-Spas, which is sortied out of the shuttle and retrieved after an independent 10-day mission. IPEX-I, performed during the STS-80 mission in December 1996, characterized the on-board dynamics of the spacecraft during normal operations and quiescent periods. IPEX-II, performed during the STS-85 mission in August 1997, monitored the microdynamic behavior of a representative 9-bay AEC-ABLE mast. The flight data demonstrates the existence of transient microdynamic events that are correlated with temperature transitions. However, the overall spacecraft flight disturbances and broadband boom stability meet the requirements of precision space optical systems.

1. INTRODUCTION

The objective of NASA's Origin Program is to address the fundamental questions of our place in the universe, such as how galaxies, suns and planetary systems form. Origins will use revolutionary new technologies to investigate these questions with a suite of new, low-cost observatories in space and on the ground. These space missions are now in the planning and definition stages, and will be launched in the beginning of the new millennium. The missions include the Space Interferometry Mission (SIM), the Next Generation Space Telescope (NGST), and the Terrestrial Planet Finder (TPF) [1] (Fig. 1).

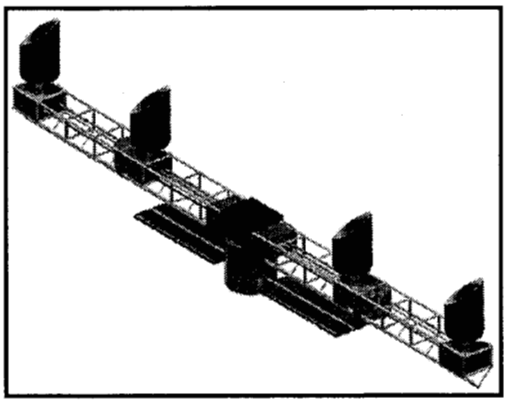

Figure 1. Terrestrial Planet Finder Design

One of the technologies that must be accomplished to meet the Origins science requirements is *nanometer* (10^{-9}m) level stabilization up to 300Hz of the optical pathlength on light weight 10-meter to 100-meter class flexible structures, in the presence of spacecraft vibrations and transient thermal distortions. Most of the disturbances will be attenuated through vibration isolation at the mechanical disturbance source (e.g., reaction wheels) and through high-bandwidth optical pathlength control of the delay lines and fast-steering mirrors. However, of concern are the quasi-random disturbances, such as thermally induced vibrations that are likely to occur when the spacecraft is subjected to large instantaneous temperature gradients or the quasi-static mechanical load redistribution when the instrument will be moving large masses. Also, the successful implementation of vibration attenuation strategies require an *a-priori* knowledge of the vibration source characteristics, of the propagation of these disturbances throughout the structure, and of the dynamic properties of the structure in its zero-g operating conditions. These disturbance models, together with structural models, are required for integrated opto-thermo-mechanical disturbance prediction, instrument design, and science requirement verification.

However, little is actually known about the high frequency broadband microdynamic behavior of large structures on orbit up to several kilohertz. Data from the Hubble Space Telescope demonstrated the existence of thermally induced snapping [2]. Some microgravity surveys were performed on orbiting space platforms, such as EURECA [3]. However, the objective of

those measurements was to characterize the low-frequency behavior below 5HZ for verification of the microgravity science requirements.

The *Interferometry Program Experiments*, IPEX-I and IPEX-II, took advantage of two ASTRO-SPAS (***S**huttle **PA**llet **S**atellite*) flights, scheduled off STS-80 (November 1996) and STS-85 (August 1997) to gain more knowledge on the broadband mechanical and thermal behavior of actual space structures on orbit. The reusable science satellite, ASTRO-SPAS (A/S), is a spacecraft developed by MBB Deutsche Aerospace, which is launched into Earth orbit by the Space Shuttle and deployed for a free flight period of approximately 10 days. At the end of its mission, the A/S is retrieved into the Shuttle and returned to Earth. The A/S is designed as the primary structure for precision optical instruments and can accommodate telescopes with dimensions up to 1.2m diameter and 3.9m length; additional small instruments can be mounted on the top or side of the pallet. The main structure of the A/S is roughly 4.6 ft x 14 ft x 2.3 ft, as shown in Figure 2. The total payload mass can reach 1800 kg, with an integrated satellite system mass of up to 3600 kg. The A/S is a low weight, high stiffness frame made out of carbon fiber compound tubes and titanium nodes, with standardized aluminum mounting panels for subsystem and payload equipment. Passive thermal control is achieved via radiation and conduction through multi-layer insulation blankets. The A/S has a 3-axis-stabilized gyroscope control system with precision star trecker as reference for pointing accuracy below 5 arcsec to astronomical targets. Twelve cold gas thrusters of 100 mN each are used for attitude control. Two thruster blocks are attached at the +Y and -Y ends of the structure as shown in Figure 2. The third is located at the keel under the platform. The thrusters apply a 100 mN pulse with a maximum duration of 200 msec and a minimum duration of 25 msec. The on-board attitude control systems automatically determines the pulsing direction and duration. A manual override exists, which allows the user to define the thruster firings for specific maneuvers. The A/S is powered by modular Li-SO_2 lithium battery pack of units of 10kWh each, for a total of 20 to 50 kWh for the payload depending on the mission duration. The flight data is directly recorded onto magnetic tapes, which is then retrieved and processed when the A/S returns to Earth. The A/S is controlled from its own operations center at Kennedy Space Center (KSC) using the Shuttle as relay station for the command and the telemetry link.

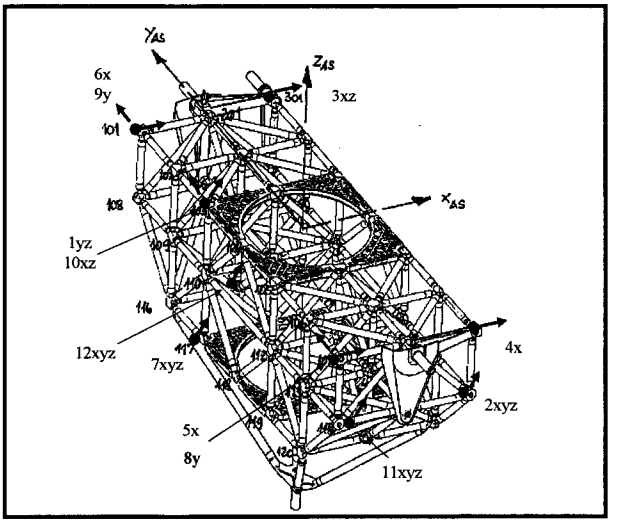

Figure 2. ASTRO-SPAS Frame with IPEX-I Accelerometer Locations

NASA and the German Space Agency DARA GmbH have agreed to perform at least 4 joint missions with the A/S system. The third SPAS mission on STS-80, named "ORFEUS-SPAS" carried the German Ultraviolet telescope ORFEUS for hot star observations as the core payload, with the NASA/JPL IPEX-I as one of its payload complement. IPEX-I characterized the vibrational environment of the A/S platform itself to determine whether it would meet the broadband nanometer stability requirements of a potential SIM technology demonstration flight. The last SPAS mission on STS-85, named "CRISTA-SPAS" carried the German CRISTA cryogenic spectrometer telescope for mapping of the Earth's upper atmosphere, with the NASA/JPL IPEX-II as one of its other payloads. During IPEX-II, a nine-bay joint-dominated pre-loaded truss was cantilevered off the side of the CRISTA-SPAS. The boom was instrumented with accelerometers, load cells, thermistors and shakers for complete on-orbit dynamic and thermal characterization of a potential Origins structural element.

2. IPEX-I

2.1. IPEX-I Experiment Design and Objectives

IPEX-I was designed to record the A/S accelerations during two orbits. The objective was to evaluate the on-board disturbances during normal operating conditions and during a prescribed quiet time when the thruster firings are stopped. The expected microdynamic disturbances are those induced by the gyros, flight data recorders (DAT) and the thrusters. Of importance are also the thermally induced vibrations, or "snap-crackle and pop". These may occur because of the mismatch in the coefficients of thermal expansion (CTE) between the graphite-epoxy frame, the titanium node connectors and the aluminum panels, which causes internal load redistribution. The thermally induced vibrations will be monitored during periods of thruster shutdown.

Approximately 229 minutes of acceleration time histories from twelve micro-g accelerometers were recorded and analyzed. The data was used to:

1) Characterize each on-board mechanical disturbance identified in the flight log
2) predict boom response levels for IPEX-II,
3) observe the structural behavior as the A/S goes through sun and shade transitions and determine whether thermal snaps exist,
4) correlate disturbance levels to ground tests and finite element model predictions.

The model used in the finite element analysis was provided by DASA, as shown in Fig. 2 with the twelve accelerometer locations and direction marked. The reduced order model has 55 nodes (one for each node ball in the frame structure) and 330 degrees of freedom which include the ORFEUS telescope and IMAPS telescope.

The micro-g accelerometers used were Sundstrand model QA-2000 sensors with a built-in temperature sensor. The data sampling system (DSS) provided 12-bits of accuracy, with a sampling rate of 745 Hz and a second-order anti-aliasing filter at 372.5 Hz. Eleven of the twelve sensors were calibrated to read 50 mg peak-to-peak and the twelfth was set at 1 g peak-to-peak. The sensor noise levels are approximately 9 μg between DC and 10 Hz, and 80 μg between 10 Hz and 500 Hz. Data was successfully recorded for all 12 accelerometers from the IPEX-1 acquisition system. The 9 μg to 50 mg window was sufficient to capture the on-orbit dynamics, since none of the recorded time histories appeared to be clipped or measuring bit noise. The largest acceleration recorded over all channels, except Channel 4, is less than 25 mg. Channel 4 had calibration anomalies and its data will not be presented herein.

2.2. IPEX-I Flight Results

The flight data has been analyzed in detail in Ref. [4]. The main events of the first orbit include a quiet time during which the thrusters were continuously on, 1 day/night transition, and 1 night/day transition. The mechanical disturbances applied to the A/S during the first orbit include the gyros, the data recorders, the IMAPS telescope, and the thruster nozzles. The second orbit includes a 3-minute quiet period where the thrusters were intentionally inhibited, 1 day/night transition, and 1 night/day transition. The mechanical disturbances for the second orbit remain the same with the exception of the IMAPS telescope that was not operational. The environment during the quiet time represents the minimum noise floor without any thruster input. During this time, the measured response can be considered a stationary, ergodic random process and the response can be quantified in terms of acceleration RMS values, peak accelerations, PSD's, and residual motion.

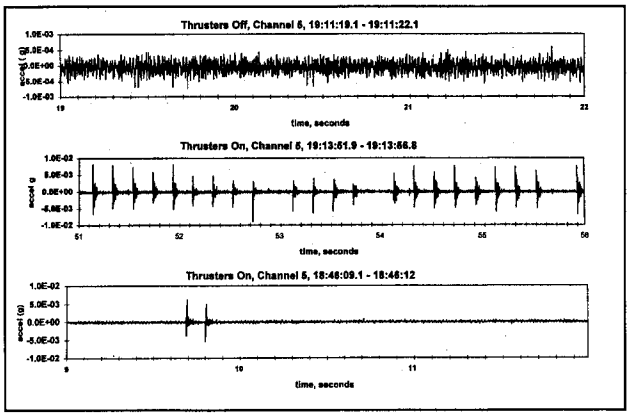

Figure 3. Typical Acceleration at Channel 5: a) Quiet Period, b) High Thruster Activity, c) Nominal Activity

2.2.a. Thruster and Gyro Activity

The dominant disturbance to the A/S platform is from the thruster firings. There are 3 sets of thruster assemblies located at each end of the structure and at the bottom of the keel. By comparing the thruster command log and the time of the event measured from the acceleration data, it was concluded that the disturbance resulted from the opening and closing of the mechanical valves on the nozzle, rather than from the acceleration due to the gas release. A sample of the measured accelerations in shown in Figure 3 for Channel 5, located at one end of the A/S and near an activated thruster assembly. The data includes 3-second time period where (a) the thrusters are turned off; (b) the thruster firings are more frequent, and (c) the thruster firings depict nominal operation modes. During these periods, the gyros and recorders were functioning and contributing to the background disturbances

The acceleration RMS values for the 3-second time period 19:09-19:12 during the second orbit when the thrusters were *OFF* are presented in Table 1, and shown in Figure 3a for Channel 5. The values presented in Table 2 are extracted from the time period 18:29-18:34 when the thrusters are *ON*.. The RMS values for the discrete frequency bands are obtained by integrating the PSD curve. Hence, the computed RMS values may also be conservative because of aliasing. Disturbances above the IPEX-I flight system Nyquist frequency of 372.5 Hz will appear aliased at a lower frequency in the PSD's and will then be included in the integrated RMS values. In particular, the A/S ground test data presented in Ref. [3], and summarized in Table 3, identified gyro disturbances at 800 Hz and 500 Hz which are aliased down to 55 Hz and 245 Hz, respectively. Gyro

disturbances are predominant in channels 1, 5, 8, and 10, closest to the gyro (Fig. 4 and 5, Table 1 and 2). To provide a more realistic set of RMS values, a second set was calculated with the gyro frequencies were filtered out at 55 and 245 Hz.

With the aliased gyro effect removed, the RMS disturbance levels of the A/S and its payloads with the thrusters off, are approximately 15 μg for [0-10] Hz, and 150 μg [0-372.5] Hz. These numbers do not include Channels 1 and 10, which are collocated on the top of the spacecraft, next to the support panels for the Orfeus telescope. The PSD for Channel 1, shown in Fig. 4, displays large resonances between 150 Hz and 200 Hz, which do not appear in the other channels and could be attributable to resonances in the adjacent support panels. This results in broadband RMS values of about 300 μg. The quietest channels, 2, 3, 9, and 12 are approximately 90 μg broadband (Tab.1). The aliasing effects of the gyros are the greatest at Ch. 7 with RMS increases of 60 μg for [10-100] Hz (Tab.1, Fig. 6).

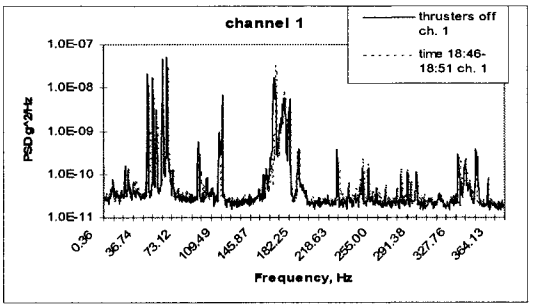

Figure 4. Typical PSD (g2/hz) at Channel 5, for thrusters- on and thrusters-off phases.

However, the thruster nozzles remain the most significant source of mechanical disturbances in the spacecraft. This is reflected by the increased RMS values between the thrusters off and on period (Table 1 and 2), and is especially true for Channels 5 and 8, which are located nearest the thruster nozzles, and for which the broadband RMS has increased by approximately 100 μg. This is also illustrated in Fig. 4, where the PSDs of Channel 5 during the thrusters on and off period are superimposed. Of course, computing a PSD for a transient signal is not mathematically correct since the pulsing sequence is neither random nor periodic in nature, however, it provides a visual representation of the frequency content of the disturbance. The relays impact the structure like an impulse, thus supplying a broadband excitation and increasing the PSD floor level. Some of that increase in the noise floor may be due to aliasing. Channels that are located away from the thruster assembly at the +Y end of the structure, such as Channel 3, 6, 7 and 9, did not display a significant change in the PSD (Fig. 6). Whereas, all channels located near the –Y end of the structure, such as channels 2, 5, 8, and 11 saw significant increases. It is suspected that nonlinear mechanisms, such as joint friction and material damping, attenuate the pulse propagation along the structure.

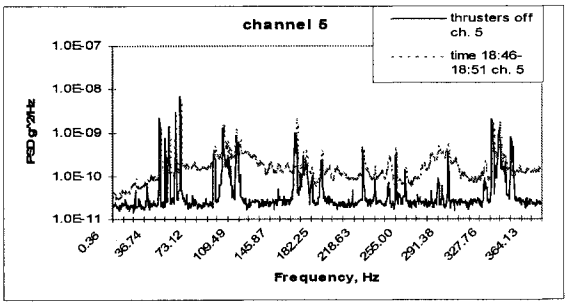

Figure 5. PSD (g2/hz) at Channel 1, for thrusters- on and thrusters-off phases of the mission.

Another way of characterizing flight data is with residual motion, as shown in Fig. 7 for Channel 5. Residual motion is computed using the reverse cumulative displacement RMS and represents the necessary controller bandwidth to achieve the desired stability requirement. This information is important when designing structures with high stability requirements, such as SIM. The plots presented here are calculated for a

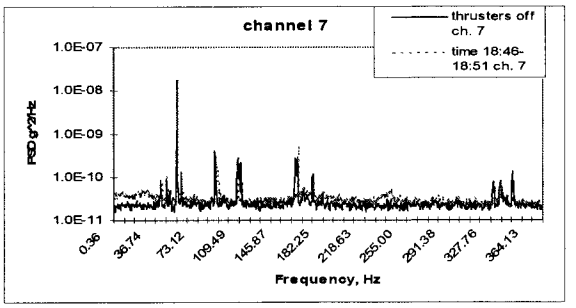

Figure 6. PSD (g2/hz) at Channel 7, for thrusters- on and thrusters-off phases of the mission.

Ch	0-10 Hz		10-100 Hz		100-372.5 Hz		0-372.5 Hz	
	w/ gyro	w/o gyro	w/ gyro	w/o gyro	w/ gyro	w/o gyro	w/ gyro	w/o gyro
1	18	18	303	254	273	273	408	373
2	14	14	47	43	76	75	90	88
3	14	14	47	46	80	79	93	93
5	14	14	117	109	141	141	184	179
6	16	16	54	53	90	90	106	106
7	15	15	115	53	88	87	145	103
8	16	16	86	70	126	125	153	145
9	13	13	42	40	73	72	85	84
10	20	20	162	109	197	197	256	226
11	15	15	48	47	100	100	112	112
12	14	14	46	44	82	82	95	94

Table 1. Astro-Spas On-Orbit Disturbance RMS with Thrusters Off, in units of μg.

Ch	0-10 Hz		10-100 Hz		100-372.5 Hz		0-372.5 Hz	
	w/ gyro	w/o gyro	w/ gyro	w/o gyro	w/ gyro	w/o gyro	w/ gyro	w/o gyro
1	19	19	286	244	257	257	385	355
2	30	30	87	84	133	133	161	160
3	14	14	48	44	84	84	98	96
5	19	19	154	147	231	232	279	275
6	17	17	56	53	94	94	111	109
7	20	20	119	56	94	94	153	111
8	35	35	147	139	172	171	229	223
9	18	18	56	53	86	85	104	102
10	21	21	167	109	189	189	253	219
11	21	21	66	63	131	131	148	147
12	15	15	50	46	95	95	108	106

Table 2. Astro-Spas On-Orbit Disturbance RMS with Thrusters On, in units of μg.

period of time where the thrusters remain open in Orbit 1, a 5-minute period of normal operations in Orbit 1, the specified quiet time in Orbit 2, and a 5-minute period of normal operations in Orbit 2. In general, the response during the first orbit for normal operations is higher than in the second orbit, since the active thrusters were located closer to Ch. 5. Figure 7 indicates that a 300 Hz bandwidth controller would be needed during nominal thruster operations to attenuate the motion down to 10 nanometers.

2.2.b. Other Disturbances

The slewing maneuvers and transitions have no noticeable effect on the time histories. The only event that is clearly evident in the time histories is when the thrusters are turned off and on.

The sun transitions occur during the second orbit at 19:16 for the day/night transition and 19:51 for the night/day transition. None of the channels show evidence of a thermally induced response or snapping when the platform moves into or out of complete shade.

An impulse appears in Channel 3 at time 19:09:26 when the thrusters are turned off (Fig. 8). The acceleration shows a peak and decay ring down typical of a structural response to an impulse-like excitation. The magnitude is 2 mg peak-to-peak. It does not occur during a sun/shade transition or a sudden change in thermal environment. Also the IMAPS telescope was not operational during this recorded orbit. No other channels show a similar response at this time.

DISTURBANCE SOURCE	FREQUENCY	EFFECT ON BOOM
GYROS	505 Hz	0.2mg RMS added by 800 Hz
	800 Hz	spike to x-dir. response of boom tip
TAPE RECORDERS	>600 Hz	Negligible
THRUSTERS	Impulse	1 mg RMS at boom tip?
CRISTA TELESCOPE	>500 Hz	~0.1 mg RMS contribution to interface
		strut response (during grating operation)
MAHRSI TELESCOPE	Multiples of 100Hz	0.2 mg RMS contribution to interface struts

Table 2. Summary of Mechanical Disturbances Observed During IPEX-II Ground Integration Tests [3].

3. IPEX-II

3.1. IPEX-II Experiment Design and Objectives

The data obtained from IPEX-I was then used to estimate the background disturbances for the follow-on flight experiment, IPEX-II, flown on STS-85 in August 1997. In IPEX-II, a 9-bay AEC-ABLE Deployable Articulated Mast boom (ADAM), constructed from graphite composite and steel fittings, was cantilevered of the side of the A/S. The boom was launched pre-deployed to avoid mechanical contamination from latch and deployment mechanisms (Fig.9). The objective of the IPEX-II experiment is to quantify the microdynamic stability of a potential structural element of an Origins structure. As in the case of IPEX-I, the prime concern is the existence of thermally induced snapping. Since the joints of the IPEX-II boom are heavily pre-loaded, the common belief prior to the flight, was that snaps should not occur. Secondary objectives are the determination of the dynamic properties of the boom on-orbit and the propagation attenuation of known mechanical disturbances.

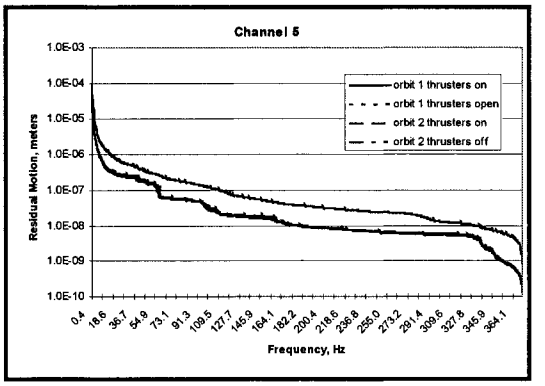

Figure 7. Residual Motions at Channel 5 for Thrusters on and off conditions.

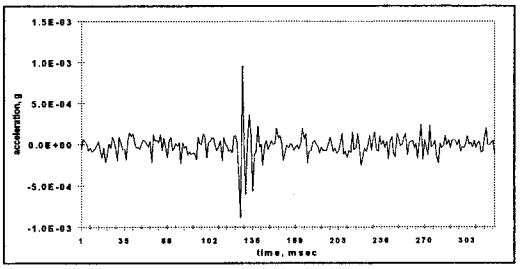

Figure 8. Anomalous Impulse at Channel 3.

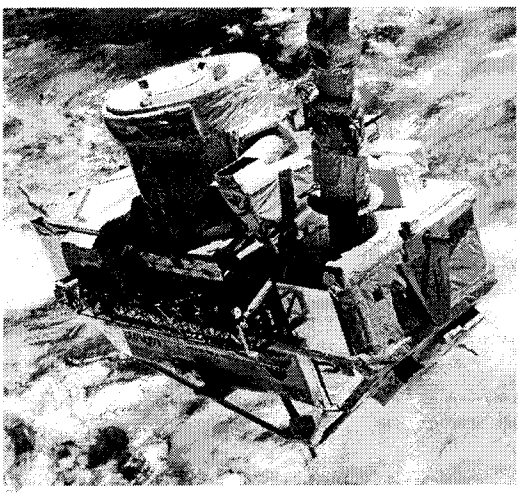

Figure 9. IPEX-II boom on-orbit

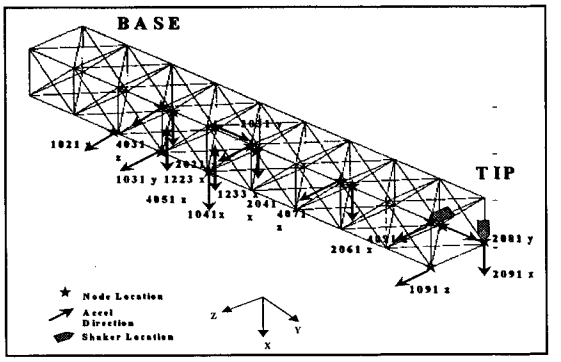

Figure 10. IPEX-II Instrumentation Layout.

To meet these objectives, the instrumentation included 24 micro-g Sundstrand QA200accelerometers, 8 load cells, 42 temperature sensors, and 2 proof-mass shakers (Fig. 10). A set of 6 accelerometers and 6 load cells were collocated inside the boom-to-spacecraft interface struts to characterize the 6 interface degrees-of-freedom. Sixteen accelerometers were installed along the boom, including 2 that were collocated with the 2 shakers and load cells at the tip of the boom. The shakers performed on-orbit modal tests to characterize the linearity and modal properties of the boom. The remaining 2 accelerometers were installed on the A/S to detect the source of the vibrations measured on the boom. The 48 temperature sensors were installed on the IPEX-II boom, of which 24 were inside the accelerometer casing for calibration purposes, 22 were collocated with the accelerometers to monitor the ambient temperature in the event of a thermal snap, and 2 were on either side of a boom strut to investigate thermal gradients across a structural member. Close to 50 hours of on-orbit data was recorded at a 1Khz sampling rate with 16-bit accuracy. Currently, the noise floor is estimated at 22μg. The on-orbit tests will be followed by a suite of ground experiments and analyses performed at JPL, MIT and the University of Colorado at Boulder.

3.2. IPEX-II Mechanical Description

IPEX-II is an AEC-ABLE 9-bay ADAM boom that measures 2.3mx0.3mx0.3m. It is assembled of CFRP graphite battens and longerons, 440C steel ball fittings at the end of the struts, and 302/304 CRES steel cable diagonals with ball end-fittings to provide pre-load to the joints (Fig. 11). The ball joints rest in spherical socket with a nominal pre-load of 275 lbs. ± 25 lbs. The boom is launched pre-deployed, and the deployment clasp mechanisms within the cable pulley assemblies are restrained against motion with 2 fasteners. The boom is cantilevered to the side of the A/S with 6 interface support struts (Fig. 12). Five of the support struts are made of graphite epoxy, and are less than 32" long. The sixth strut is made of titanium and is 4" long. The support struts are attached to the boom through an invar end plate to minimize CTE (coefficient of thermal expansion) mismatch between the struts and the boom. Inside each of the support struts are 6 sets of collocated accelerometers and load cells to provide the full 6-dof representation of the A/S disturbance inputs into the boom. The free-end of the boom is restrained during launch and landing with a stow pin mechanisms, which is then opened during flight. The torsional rigidity of the boom is also maintained with an aluminum free-end plate through which the stow-pins passes, and to which 2 orthogonal shakers are attached to perform th eon-orbit modal tests. Thermal MLI tape is applied locally to the boom joint fittings and to the pulley plates to minimize temperature gradients. The sensor cables have service loops that minimize their stiffness coupling to the boom, and are fed down to a cable tray located just under the boom. The sensor signal conditioners are located inside the cable tray. The total mass of the boom assembly is 38.9 Kg, which includes 13.3Kg for the boom, 9.4Kg for the fixed end plate, 2.2Kg for the free end plate, 9.9Kg for the support struts, 2.6Kg for the sensors and 1.5Kg for the 2 proof-mass actuators (PMA).

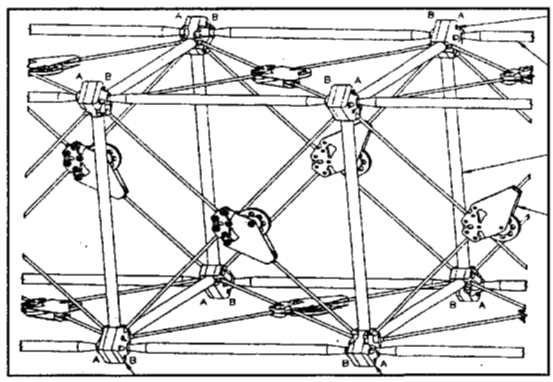

Figure 11. IPEX-II bay detail.

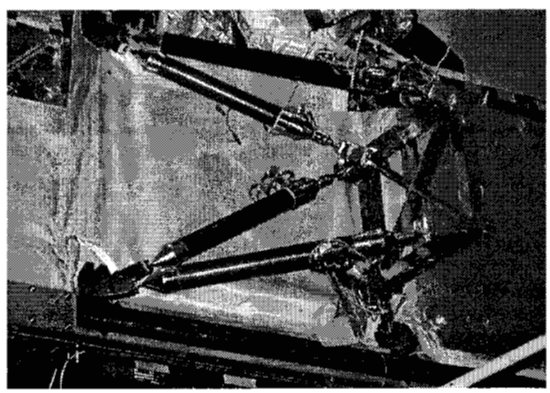

Figure 12. IPEX-II support struts.

3.3. IPEX-II Flight Data Results

The flight experiment captured data over 50 hours of on-orbit operations. The data was recorded in 5minutes blocks at 20-minute to 9-minute intervals required for data download to the tape recorders. During the first 45 hours, the data recorded the response of the boom during A/S normal operation modes, including gyros, thrusters, and other payloads. This period also included over 25 day/night and night/day transitions. Furthermore, two experiments recorded at the slower sampling rate of 909Hz to identify any aliased response. The last 5 hours of the A/S flight were specifically dedicated to IPEX, and all other payloads were turned off. The most important experiment is a 5-minute segment when even the A/S gyros and thrusters were shut down, and the boom went through a sudden night to day transition. This is the minimum disturbance state of the A/S, and is the period most likely to measure thermally induced microdynamics in the boom. There were also 14 experiments that performed multi-shaker modal tests for the purpose of assessing the on-orbit structural dynamic properties of the boom. Two experiments were also dedicated to evaluating the boom response to specific A/S mechanical disturbances: gyro response without thrusters, and dedicated thruster pulsing sequence and direction with or without the gyros in the background. These

tests will estimate the amount of disturbance propagation attenuation, a critical issue when predicting the response of the large precision structures to on-board disturbances.

More than 10 gigabytes of data has been collected during the flight experiment. At this time the data has not been completely analyzed, and the post-flight instrument calibration and verification have not yet been performed. The following is a synthesis of data that has been analyzed to date using pre-flight calibration information. A future report will update this data as necessary.

3.3.a. Thermal stability and microdynamics

At the beginning of the quiet period, during which all thrusters, gyros and payloads were turned off, the boom had been in complete shade for 1.5 hours, and the gyros had been shut down for 4.5 minutes. Except for the tape recorders, no mechanical or thermal disturbances were affecting the boom. Using the current orbital information for the A/S, a night to day transition was predicted to occur 30 seconds into the data. Figure 13 shows the temperature response of a sensor located on a strut during that experiment. The boom was originally at –40°C, and some of the initial oscillations may be due to the low-pass filter used to extrapolate the data.

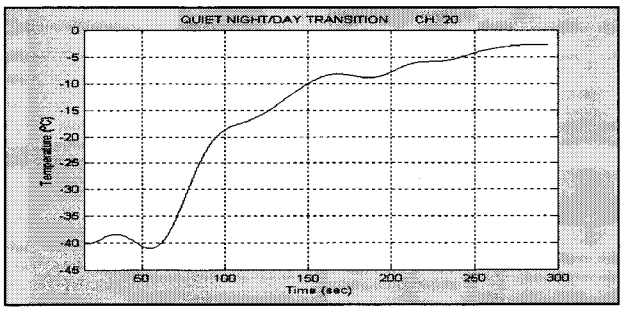

Figure 13. Temperature profile at boom mid-point during night/day transition.

However, the temperature starts rising at approximately 60 seconds into the data. It is not clear whether the delay in the temperature rise is due to a 30-second error in the transition estimate, or a self-shadowing effect of the boom onto the sensor. Then the temperature heats up rapidly, and reaches 0°C by the end of the experiment. Not all sensors show this trend because of self-shadowing and delayed temperature rises of the local material. However, by the time the next experiment starts recording, 10 minutes later, all sensors read a temperature of about 0°C. Hence, for analysis the data will be broken up into three parts, period 0sec to 30sec is the "night" data, 30sec to 70sec is the "transition" data, 70sec to 250 sec is the "transient day" data. Thrusters are activated after 250sec as shown by the two pulses, and this segment will be treated separately.

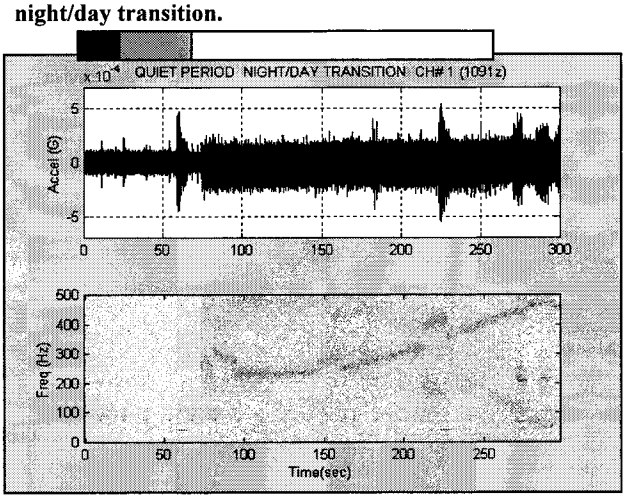

Figure 14. Acceleration time history and spectrogram at Ch. 1 (Z-dir bending at boom tip) during quiet period.

A representative signal is shown in Fig. 14, for Channel 1, which is located at the tip of the boom, and measures transverse motions in the z-direction. The top plot is the measured acceleration, the bottom plot is the time varying Fast Fourier Transform (FFT), also known as the spectrogram, and is a graph of time versus frequency where the FFT amplitude is represented by the color intensity. The spectrogram is more accurate than the power spectral density (PSD) for assessing the time varying spectral content of transient disturbances.

During the night period, spikes of about 150 μg peak-to-peak occur at 15sec intervals. These spikes are correlated on the spectrogram with activity around 100 Hz, and persist throughout the whole record. This behavior could be consistent with the disturbances from the rotating tape recorder mechanisms. During this period, the background level is approximately 35μg broadband RMS, and includes the noise floor of the instrumentation which is estimated at 22μg. The identified disturbances are summarized in Figure 15, which displays the broadband RMS (0-500Hz) over all channels as a function of the

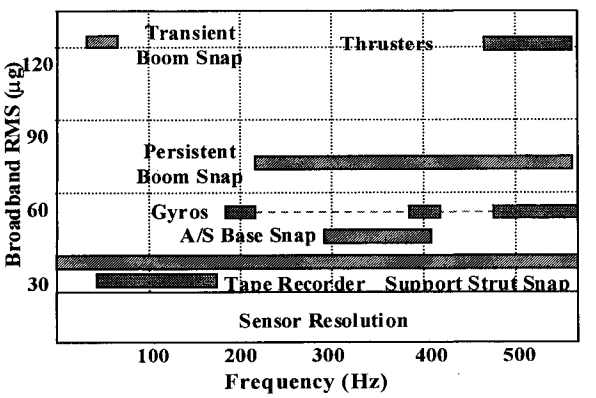

Figure 15. Summary of boom RMS disturbances and predominant frequencies observed during the quiet period.

predominant frequency content. These numbers may be revised after the post-flight calibration tests are performed.

During the transition time (30sec to 70sec), a snap occurs at 58 seconds into the data. This snap is characterized by a 1mg peak-to-peak impulse followed by a decayed ring down of a mode around 40 Hz. Pre-flight analysis predicted the fundamental torsional mode at that frequency. This transient boom snap has a RMS of about 130μg, and is the largest near the tip. Channels away from the tip do not show the impulse at the beginning of the snap, and have responses that are lower amplitude. One example is Ch.4 located in the middle of the boom, 4 bays down from the tip, and measuring x-direction motions (Fig. 16). The reduced amplitude may be consistent with the response of the boom at that location for the first torsional mode. However, the acceleration in this channel only shows a ring down without an initial impulse, with a resonant frequency of 40 Hz as indicated by the corresponding PSD. The disappearance of the initial impulse together with the local response at the structural mode is consistent with observed propagation attenuation effects of impulsive disturbances such as earthquakes. Based on the seismic analogy, the impulsive boom snap may have initially occurred near the tip of the boom. Its cause has not yet been determined. A second similar event is observed at 225sec (Fig. 14).

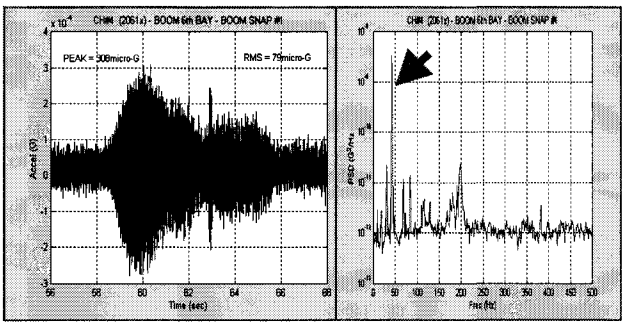

Figure 16. Impulsive boom snap at Ch. 4 (X-dir. bending in 6th bay.

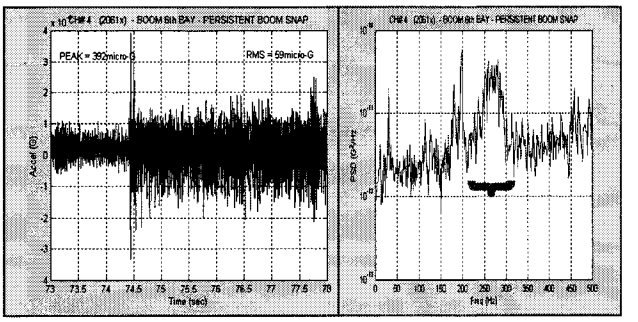

Figure 17. Persistent boom snap at Ch. 4 (X-dir. bending in 6th bay).

During the transient day period (70sec to 250sec), the signal suddenly becomes very noisy and the boom seems to be in a continuous state of crackling (Fig. 14). This crackling is observed in every channel, but completely disappears in the next experiment 10 minutes later when the internal boom temperatures have stabilized. The time 74sec corresponds to the sharp rise in temperature observed in Fig. 13. The crackling has a peak-to-peak amplitude of 400μg, and an RMS of about 75μg. This persistent boom snap is characterized by a time varying frequency which increases from approximately 250Hz to 500Hz over the course of the experiment, as shown in the spectrogram in Fig. 14. Intermittent jumps in the FFT are correlated in time with other simultaneous snapping events. It is suspected that this signal is aliased through the second order anti-aliasing filter, and the signal is in fact decreasing in frequency from 750Hz down to 500Hz. This decrease in frequency would be consistent with the rise in temperature during this period, which in turn extends the cables and decreases the pre-load at the joints. A preliminary modal test performed on a single bay article uncovered a very nonlinear mode in the vicinity of 600Hz, which could be associated with the persistent boom snaps. Persistent crackling may be a reflection of the boom adjusting to the new applied load (thermal) and redistributing its internal strains to the minimal energy configuration. In doing so, stress is relieved at the joints and at all discontinuous interfaces. It should be noted that in theory any type of load could produce this effect, including mechanical load redistribution due to moving parts. A close-up of the crackling is shown in Fig. 17 for Ch. 4, where the event is immediately preceded by one or more large impulses at 74.5sec. This initial impulse is observed in some of the other channels, but not in Ch. 1 at the tip of the boom in the Z-direction (Fig. 14). Looking at the synchronization of the pulse, it

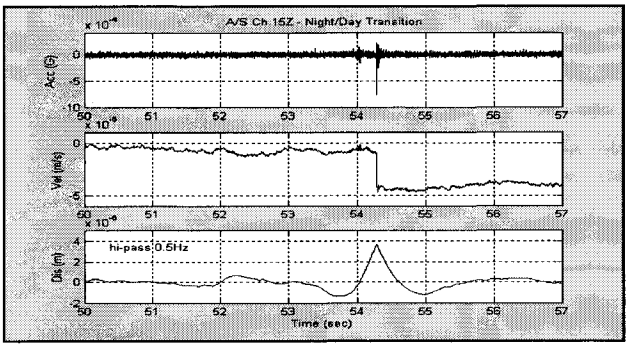

Figure 18. A/S base snap (Ch. 15).: a) acceleration (g), b, velocity (m/sec),c) displacement (m)

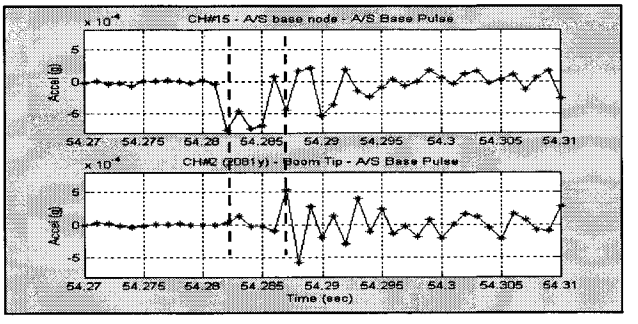

Figure 19. A/S base snap pulse propagation in axial direction from a) A/S interface (Ch.15) to b) boom tip

seems to have triggered in the bays near the base of the boom, but is largest at the boom to A/S interface. It is unclear whether the initial impulses and the crackling are related, but it is conceivable that this initial impulse triggered an internal instability within the boom.

Another significant snap occurred at 54sec, as shown in the top trace in Fig. 18 for Ch. 15, located on the A/S node to which the support struts are connected. The mechanism that produced this snap is unclear as each strut was tightly bolted down to the A/S with 7 bolts. Synchronization of this snap across the boom indicates that it initiated on the A/S side, with a delay of about 6millisec from the A/S (Ch.15) to the tip of the boom, as shown in the close-up in Fig 19. This is consistent with the first axial mode of the boom, measured at approximately 216Hz during the ground modal test, over a distance of 2.5m from the base to the tip. Also the peak-to-peak acceleration is one-sided at the A/S base with an amplitude of 0.8mg, whereas after propagation along the boom, the pulse becomes double-sided with a peak-to-peak amplitude of 1.1mg (Fig. 19, Ch. 2). One-sided acceleration pulses are typically associated with a jump in velocity, and a drift in the displacement. This is illustrated in the two bottom plots of Fig. 18. The velocity has a quasi-instantaneous jump of 50μm/s, and the associated displacement has a *relative* 6μm peak-to-peak motion. The displacement time history in this figure has been high-pass filtered at 0.5Hz to remove parabolic drifts due to unknown initial conditions.

The cable assemblies are also very active during the quiet period, as shown in Fig. 20. The time traces shown in this plot represent the first 3 minutes into the quiet period, and encompass the night, transition and transient day conditions. The channels shown are, from top to bottom, a) Ch.14 which measures the cable drum modes in the x-direction in the 3rd bay, b) Ch. 11 which measures the cable drum modes in the 4th bay adjacent to the previous channel, c) Ch. 10 which measures the z-bending of the boom at a node in between the 2 previous bays, and d) Ch. 8 which measures the axial y-motion of the boom in between the 2 bays. The main driver of the cable modes are the tape recorder pulses, as seen by the synchronization of the drum mode ring-downs with the regular 15-sec pulse (Fig. 20-c). Also, the response amplitudes are greater at Ch.14 (Fig. 20-a) than at Ch. 11 (Fig. 20-b) located further away from the A/S input. Because of disturbance attenuation over distance, this is consistent with the tape recorder disturbance assumption. Also, the cables do not respond significantly to the boom transient snap at 58sec, or the boom persistent snaps starting at 74sec. Furthermore, there are drum modes that occur in the absence of observable spikes in the boom data, such as the ring-down clusters at 110Hz and 150Hz in Ch. 14 (Fig. 20-a). This may be an indication of A/S generated disturbances that are below the noise floor of the IPEX sensors. The periodic nature of these pulse clusters suggests that they might also be linked to the tape recorder disturbances. Conversely, there are several pulses in the boom channels that do not excite drum modes. One notable example is the initial pulse at the beginning of the persistent snap period at 74sec. Hence, it might be deduced that the cables to do not respond to structural snap-like disturbances. Thus, the cable data can be used as a discriminator to detect which spikes observed in the boom response are from the tape recorders and which spikes are from structural snaps.

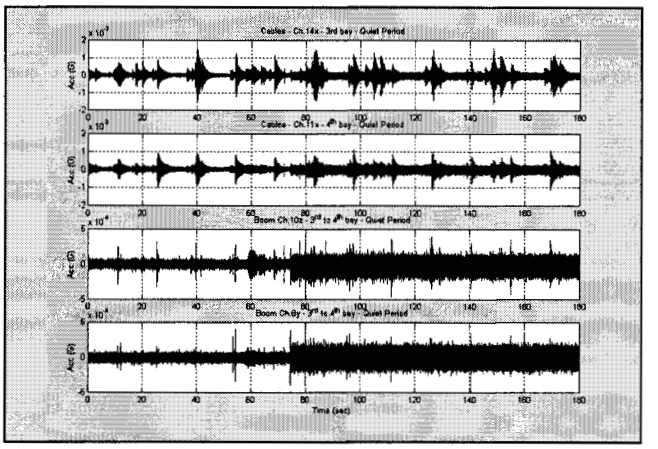

Figure 20. Cable drum modes synchronized with pulses on boom: a) Cable Ch.14x, b) Cable Ch. 11x, c) Boom Ch. 10z, d) Boom Ch. 8y.

There are still many snaps in the quiet period data that have yet to be identified. Also, the night/day transitions recorded during the A/S normal operations period need to be examined for similar snapping characteristics. These findings will be reported in the future.

3.3.b. Astro-Spas Mechanical Disturbances

The latter part of the quiet period and the following next two experiments were dedicated to characterizing the Astro-Spas induced mechanical disturbances, namely, the thrusters and gyros. During the last 30 seconds of the quiet period (270-300 sec, Fig. 14), the thrusters were activated in a particular sequence with the gyros still turned off. In the following experiments, the gyros were turned back on, and there were intermittent periods when the thrusters were pulsed. During these experiments, the boom always remained in shadow, and hence, was unperturbed by thermal disturbances. Thus, it was possible to individually characterize each disturbance source. The results are summarized in Fig. 15. The thrusters add about 120μg RMS broadband, to the response at the tip of the boom, with predominant contributions at 400Hz to 480Hz, which is aliased down from 520Hz – 600Hz as confirmed by the data sampled at 900Hz, and by the IPEX-I results. At the base of the

boom, on the A/S, the thrusters imparted a disturbance of approximately 60μg RMS. The gyros are narrowband disturbances with components at 200 Hz, 400Hz, and 495Hz. These are aliased own from 505 Hz and 800 Hz, as confirmed by the 909Hz sampling experiments, and the pre-flight ground tests (Table 3.). The disturbance is largest next to the gyros at Ch. 16 with 306μg RMS, but only measures 24 mg at the base of the boom with 50μg response at the tip. Again, propagation attenuation significantly reduced the disturbance levels of the source mechanisms. Disturbances induced by the tape recorders and the various snaps have been reported earlier, and are also summarized in Fig. 15.

As for IPEX-I, residual motions were computed for each of the thermo-mechanical disturbance sources, as shown in Fig. 21. Five different lines are drawn for the night, transition, and transient day thermal conditions, as well as for the thrusters and the gyro mechanical disturbances. The data for each line represents the RSS value of the reverse cumulative PSDs over all acceleration channels, divided by ω^4 to integrate into displacements. As expected, the night period is the quietest by a factor of 5 in certain regions. Overall, the boom is relativity quiet in an RMS sense, since above 100Hz the residual motions are less than 10 nm, and thus fit within the current SIM stability requirements. HOWEVER, it should be remembered that RMS metrics are not appropriate for transient disturbances, since they smear out any large spikes. Such low numbers do not preclude mg acceleration pulses, 50 μm/s velocity jumps and μm level instantaneous motions (Fig.18). When designing precision structures, it is strongly advised to include requirements that also specify peak allowable motions.

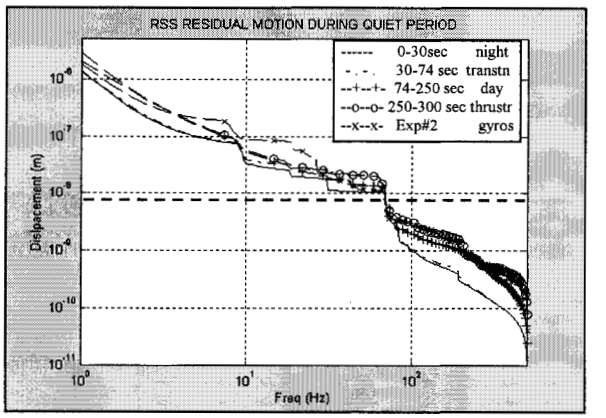

Figure 21. RSS residual motions for individual thermo-mechanical disturbance sources.

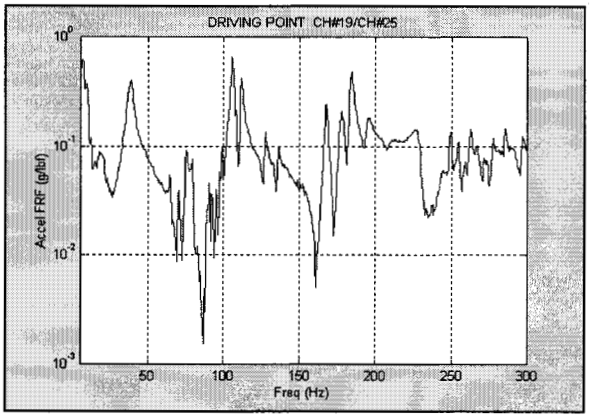

Figure 22. Driving point acceleration transfer function at shaker #1, obtained during broadband random input tests.

3.3.c. Structural Dynamic Characterization

The 2 mechanical shakers located at the tip of the boom were used to perform modal tests for on-orbit characterization of the boom dynamics. Fourteen 5-minute tests were performed, including five broadband random input tests between 9Hz and 303Hz, at two input levels of 0.101lbf and 0.0126lbf. Narrowband step-sine tests were also performed in bands of 12 Hz to 35.7Hz, 34.5Hz to 56 Hz, and 54.8Hz to 90.6Hz. Because of electronics limitations, the step size of the sine tests could not be smaller than 1.2 Hz, and each sweep could not be longer than 5 minutes. To circumvent this limitation, a new alternating step-sine testing technique was implemented, which numerically shown to provide modal property estimates for frequency and damping than the traditional step-sine technique when both step size and test times are limited.

Dynamic properties of the boom have yet to be extracted from the flight tests. However, the data was verified, and a sample acceleration transfer function is shown in Fig. 22 for the driving point at shaker #1. The experiment was a broadband burst random test between 9.5Hz and 303Hz, performed at the high force level of 0.1lb. The experiment was a total of 17 cycles over 5minutes, with 10 seconds of random shaking followed by 8 seconds off. According to pre-flight analytical predictions the large peak at 38.5Hz should be the first torsional mode. This is also the mode that was most active during the local boom snap ring-down. The damping assessed by the half-power bandwidth method is a approximately 4%. Pre-flight ground modal tests measured less than 1% damping for this mode. Some of the potential causes for the on-orbit damping increase are the frictional effects of the sensor cables or the friction of the joints in zero-g. Post-flight testing of the boom will be performed with the same cabling configuration as on orbit. This will demonstrated whether the cables were responsible for the additional damping. Assessing what mechanisms increase damping on-orbit will be important for the accurate response prediction of the precision optical systems to on-board disturbances.

3.3.d. Operating Mode Dynamics

Data from the first 45-hour period during nominal operating mode has also been examined. RMS levels have been computed for each of the channels and experiments, and compared. The data shows that during this period, when the gyros, thrusters

and all the payloads are functioning, there is a predominant mode at 216Hz that varies significantly from one experiment to next. This mode was not identified during the pre-flight systems ground tests, and does not appear during the IPEX-II dedicated experiment sequence. Hence, it is believed to be induced by one of the payloads, and most possibly the Crista telescope, which is equipped with a cryo-cooler. The 216Hz mode was filtered out of the data, since it was not related to the functionality of the spacecraft or the boom. A comparative plot is shown in Fig.23 for experiment #1-04, which was recorded during a full night sequence. The acceleration PSD for Ch. 3 at the tip of the boom is shown for reference in Fig. 24, and the RMS bandwidth decomposition is reported in Table 4 for the 216Hz data filtered out. Most of the responses are less than 150μg RMS, the few exceptions are Ch. 16 on the A/S nearest the gyros, the axial channels on the boom (Ch. 2Y), and the cable-assembly channels (Ch. 11 &14). The later is mainly due to the resonant drum modes around 80Hz.

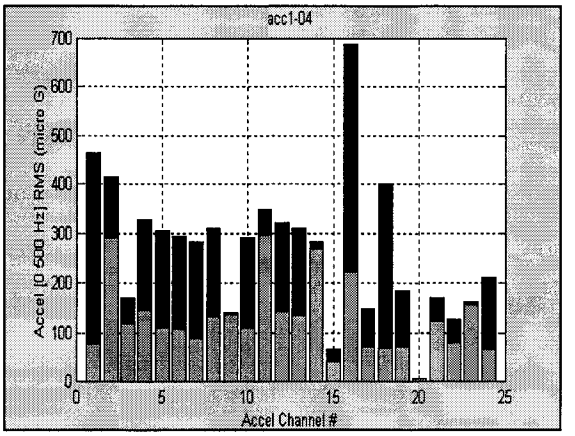

Figure 23. Broadband RMS levels computed for each accelerometer location, for night experiment #1-04. (Dark bar: unfiltered data, Light bar: 216Hz removed)

Two separate experiments during the nominal period were run at a slower sampling rate of 909Hz. Figure 25, compares the PSDs for Ch. 15 on the A/S at the boom connection node. The top PSD is for Exp. #1-01 sampled at 909Hz, and the bottom PSD is for the subsequent experiment Exp. #1-02 recorded at 1000Hz. The 91Hz differences between the two plots clearly illustrate the aliased frequencies in the data. In particular the 800Hz gyro mode is aliased down to 109Hz and 200Hz respectively, the 505Hz gyro mode is aliased down to 404Hz and 495Hz respectively. Although aliasing is generally a problem, here aliasing is a tool that will be used to track higher frequency modes such as would be expected during a snap.

	RMS (μG) per FREQUENCY BANDS (Hz)						
CH	0-10 Hz	10-100	100-200	200-300	300-400	400-500	0-500
1	5.55	37.4	32.2	37.8	16.9	45.9	79.3
2	4.29	16.3	34.8	82.5	41.0	249.4	268.7
3	4.09	31.6	74.8	57.2	28.1	89.8	136.8
4	3.70	20.1	84.1	30.8	31.6	54.8	111.5
5	6.82	31.3	48.4	52.1	37.3	73.3	113.4
6	8.89	23.7	40.8	52.2	27.3	103.3	128.3
7	9.74	21.8	29.6	51.2	34.9	70.6	101.3
8	9.08	26.8	41.9	55.1	35.5	108.7	136.7
9	5.36	30.0	75.9	40.8	42.1	111.4	150.1
10	4.42	24.6	86.6	34.3	38.2	82.8	132.7
11	10.05	170.7	79.5	58.1	13.2	15.1	198.4
12	9.48	19.3	74.0	49.4	23.5	89.7	130.3
13	6.58	23.3	88.2	69.6	28.4	87.5	147.2
14	5.94	225.8	144.5	25.9	11.5	15.6	270.1
15	5.03	14.7	17.4	14.8	21.8	13.9	37.8
16	18.40	127.6	90.2	71.9	168.0	86.1	256.0
17	4.09	23.9	34.7	36.9	15.5	46.3	74.5
18	3.82	23.0	32.4	32.4	13.4	44.8	69.5
19	4.62	18.8	40.2	34.0	22.7	53.1	80.5
21	8.52	67.6	77.1	36.1	53.6	59.6	135.3
22	4.71	33.9	45.2	24.7	34.5	53.7	88.9
23	5.81	61.6	70.5	50.0	96.2	65.0	157.4
24	5.88	14.3	36.0	30.8	25.6	36.4	66.9

Table 4. RMS (μg) for night experiment #1-04 as a function of channel location and bandwidth, with 216Hz filter applied.

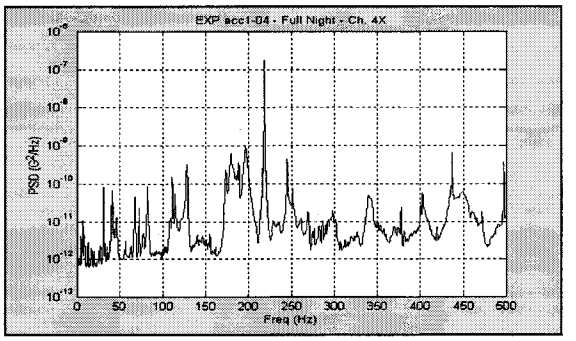

Figure 24. PSD of Boom Ch.4X for Exp.#1-04.

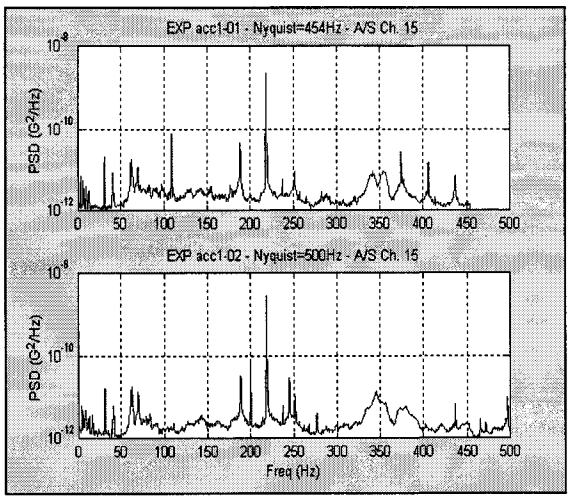

Figure 25. Aliasing: PSD of A/S Ch.15 at boom interface for Exp.#1-01 with 909Hz sampling rate, and Exp.#1-02 with 1000Hz sampling rate.

4. CONCLUSION

The IPEX experiments demonstrated the high-frequency nanometer thermo mechanical stability of the ASTRO-SPAS platform and a representative boom on-orbit. Preliminary data indicates that all the instrumentation functioned as planned during the flight, and that the IPEX experiments were successful. The broadband acceleration RMS levels both on the ASTRO-SPAS and the boom were in the hundreds of micro-G's, thus confirming their suitability for Origins-class payloads. Analyses have been performed that assess the disturbance contributions for spacecraft mechanisms such as gyros and thrusters, as well as thermal disturbances.

Also, propagation attenuation of ***transient*** disturbances was shown to significantly decrease in amplitude and change in aspect away from the source. This may be a direct result of wave dispersion effects, as well as the higher damping observed on-orbit. Thus, implying that transient disturbances would mostly impact mechanical and optical components located in the vicinity of the disturbance source. Furthermore, it has been shown that traditional spectral methods are not appropriate to gauge the intensity of the transient disturbances. Some snaps have been shown to have large instantaneous velocities and micron displacements, while not significantly perturbing the μg RMS levels. All these issues are important when designing vibration attenuation strategies and predicting performances of sensitive opto-mechanical elements.

Foremost, IPEX demonstrated the existence of internal snaps in a pre-loaded joint-dominated structure, thus invalidating conventional wisdom which dictated that preload prevents all motion and stabilizes the microdynamics. It was noted that temperature variation is only one of the ways load is internally imparted to a structure. In theory, internal mass and inertia redistribution due to moving elements could trigger the same microdynamic snap mechanisms. It was also shown that internal snaps are not all lurch-like events with single-mode ring down. Some microdynamic events are persistent, others occur prior to an abrupt thermal load variation, and others initiate away from the boom near the bolted interface connections. These observations are not unlike the phenomena observed after earthquakes, with aftershocks occurring years later on unconnected faults. Although the source of these specific snaps has yet to be identified and modeled, it is suspected that they occur along discontinuous contacting surfaces [6]. This is not restricted to the joint-dominated truss architecture of the IPEX boom. Discontinuous surfaces are also prevalent in composite structures, which are known to snap under thermal cycling.

Nevertheless, the IPEX data demonstrated that even in the presence of microdynamic events, the ASTRO-SPAS spacecraft and the AEC-ABLE ADAM mast boom provide the level of stability required for future Origins mission, and as such, establish a cornerstone for all future precision optical space system designs.

Continued analyses of the flight data, as well as modeling and ground test validation of observed space microdynamic events, in support of NASA's Origins missions, will be the emphasis of the future work performed under the Microdynamics Interferometry Technology Program at JPL.

5. ACKNOWLEDGEMENTS

This work was performed at the Jet Propulsion Laboratory, California Institute of Technology, under contract with the National Aeronautics and Space Administration. The author would like to thank R. A. Laskin, Interferometry Technology Program, and the IPEX team of JPL, as well as the DASA ASTRO-SPAS team at KSC for their guidance and commitment of resources that made this work possible.

6. REFERENCES

1. Naderi, F., "NASA's ORIGINS Program", Paper **3350-125**, *Proc. SPIE Astronomical Telescopes and Instrumentation Conference*, Kona Hawaii, March 1998, (to be published).

2. Blair, M., and J. Sills, "Hubble Space Telescope On-Orbit System Identification", *Proc. 12th International Modal Analysis Conf.,* Honolulu, Ha, Feb 1994, p. 663-669.

3. Eilers, D., U. Lubbers, and F. De Rose, "EURECA-MMS Microgravity Measurement Subsystem Post-Flight Evaluation, Final Report", ESA/ESTEC Contract report N0. 10016, Bremen Germany, Dec. 1994.

4. Levine, M, and R. Bruno, "Interferometry Program Experiment #1: Flight Data Analysis", NASA Jet Propulsion Laboratory Document **JPL D-14904**, Pasadena CA, (to be released).

5. H. Gutierrez and M. Levine, "Analysis of IPEX-2 Pre-Flight Ground Integration Test Data", ", NASA Jet Propulsion Laboratory Document **JPL D-14905**, Oct. 1997, Pasadena CA, (to be released).

6. Warren, P., and L. Peterson, "Sub-Micron Mechanical Stability of a Prototype Deployable Space Telescope Support Structure", **A97-1375**, *Proc. 38th AIAA/ASME/ASCE/AHS/ASC Structures, Structural Dynamics, and Materials Conference*, Kissimmee, FL, Apr. 7-10, 1997; p. 2890-2899.